

# Current-Carrying Characteristics of Conductive Microfiber Electrical Contact for High Frequencies and Current Amplitudes: Theory and Applications

Annette Muetze, *Senior Member, IEEE*, and H. William Oh, *Member, IEEE*

**Abstract**—Rings made from millions of conductive microfibers, if designed properly, have shown to be a good electrical contact for applications that require high frequencies and high current amplitudes while minimizing the problems of excessive wear and hot-spotting/thermal wear commonly encountered with conventional sliding contacts. In this paper, we describe the current-carrying characteristics of such rings for high frequencies up to several megahertz and large current amplitudes of several tens of amperes. We develop the theory to understand these characteristics, and thus the ring design, and support and illustrate the theoretical findings with experimental results.

**Index Terms**—Bearing current, common-mode current, electric field effects, electromagnetic interference (EMI), variable-speed drives.

## NOMENCLATURE

AC	Alternating current.
DC	Direct current.
EMI	Electromagnetic interference.
HF	High frequency.
$a_c$	Contact spot area.
$a_s$	Radius of the microfiber shaft.
$c_1$	Proportionality constant in eq. describing $R_f(i)$ .
$c_2$	Exponential constant in eq. describing $R_f(i)$ .
$C_{wf}$	Stator winding-to-frame capacitance.
$d_{al}$	Average diameter of the aluminum ring.
$d_{shaft}$	Shaft diameter.
$d_{2mfrs}$	Separation between the two microfiber rings under test.
$f$	Frequency.
$i$	Current.
$i_b$	HF circulating bearing current.
$i_{com}$	Common-mode current.
$I_b$	Amplitude of $i_b$ .
$I_{com}$	Amplitude of $i_{com}$ .
$l$	Length of the microfiber shaft.

$n$	Motor shaft speed.
$R_f$	Microfiber resistance.
$R_{f1}$	Resistance of an individual microfiber.
$R_{al,ring}$	Resistance of aluminum ring.
$R_{al,shaft}$	Resistance of aluminum shaft between the two microfiber rings.
$R_c$	Constriction resistance.
$R_{c,x}$	Constriction resistance for x microfibers conducting in parallel.
$R_{ring}$	Resistance of the microfiber ring.
$R_s$	Resistance of the microfiber shaft.
$R'_s$	Resistance of the microfiber shaft per unit length.
$R_{s,x}$	Resistance of the microfiber shaft for x microfibers conducting in parallel.
$s_b$	Distance the fibers travel during the time $t_b$ .
$t$	Time.
$t_b$	Time for a current-conducting bridge to develop.
$t_{zc}$	Time between two zero-crossings = $T/2$ .
$t_{mm}$	Time between two maxima of the source behind the current at maximum field strength.
$T$	Period time.
$v$	Velocity at the shaft surface.
$v_{Lg}$	Voltage between motor terminal and ground.
$\delta$	Skin depth.
$\delta_{al}$	Skin depth of aluminum.
$\mu$	Permeability.
$\rho$	Specific resistivity.
$\rho_{cu}$	Specific resistivity of copper.

## I. INTRODUCTION

MODERN power-electronics-based drive technology has brought a wide variety of inverter-operated machines and actuators. Depending on the application and hence the design, the drives can have excellent control and variable speed performance, and can potentially offer significant energy savings when compared to conventional systems. The advent of these modern drive systems that often use fast-switching inverters with high  $dv/dt$  has brought forth a variety of parasitic phenomena. These have seen a lot of attention both from academia and from industry and include, for example, high-frequency (HF) ground leakage currents (e.g., [1]–[3]), HF shaft voltages and bearing currents (e.g., [4]–[16]), electromagnetic interference (EMI), and the need to develop appropriate filtering techniques (e.g., [17]–[23]). Appropriate handling of these phenomena has become an important element during the design of power-electronics-based drive systems to avoid damage to

Manuscript received November 20, 2009; revised February 16, 2010. Date of current version July 16, 2010. Recommended for publication by Associate Editor B. Lehman.

A. Muetze is with the Institute of Electric Drives and Machines, Graz University of Technology, 8010 Graz, Austria (e-mail: muetze@tugraz.at).

H. W. Oh is with Electro Static Technology, Mechanic Falls, ME 04256 USA (e-mail: hwoh@est-static.com).

Color versions of one or more of the figures in this paper are available online at <http://ieeexplore.ieee.org>.

Digital Object Identifier 10.1109/TPEL.2010.2046499

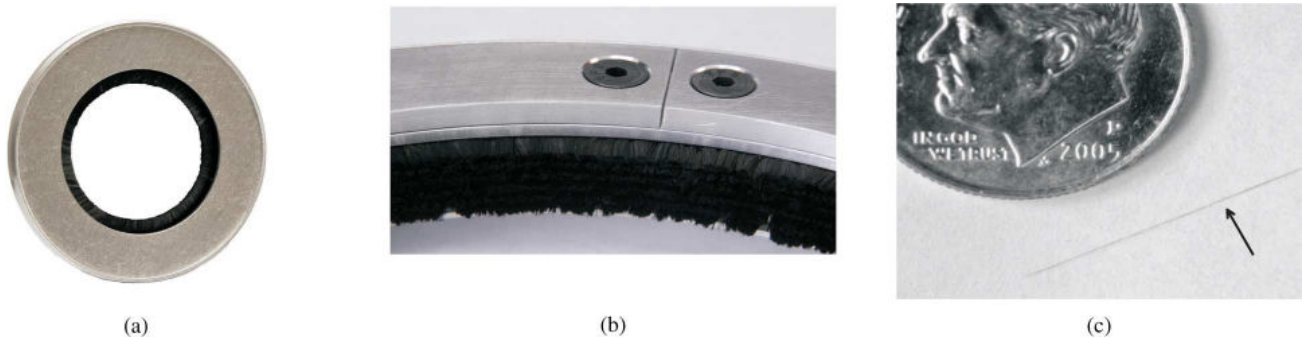


Fig. 1. Examples of multitudes of conductive microfibers assembled to give conductive microfiber rings and microfiber bundle. (a) Example of a smaller microfiber ring. (b) Close-up view of a larger microfiber ring. (c) Bundle of microfibers.

the drive system and its operating environment. In this context, electrical contacts for sliding contact interfaces have also become of renewed interest. Rings made from millions of conductive microfibers, if designed properly, have shown to be a good electrical contact for applications that require high frequencies and high current amplitudes while minimizing the problems of excessive wear and hot-spotting/thermal wear commonly encountered with conventional sliding contacts. Such microfiber rings thereby present a cost-effective option for a mitigation technique for inverter-induced bearing currents. However, this example should not obscure any other context in which current conduction of HF signals across sliding contacts can be required, such as minimization of EMI emitted from rotating machinery, e.g., in the presence of sensitive electronics or sensors, or to meet military EMI requirements. This paper contributes to the development and use of alternative electric contact mechanisms across sliding surfaces, notably for HF applications with larger current amplitudes.

In previous papers, we have focussed on electric charge dissipation [24] and general design aspects [25]. Here, we explicitly concentrate on the current-carrying characteristics of such microfiber rings, focusing on high frequencies up to several megahertz and large current amplitudes up to several tens of amperes, in contrast to low frequency and dc signals. These characteristics and the influence of the different operating parameters, such as not only current amplitude but also current frequency and motor speed, has previously not been analyzed in detail. However, such a quantification is highly important to fully take advantage of the benefits such microfiber rings can offer. For completion, we first review briefly the microfiber ring concept (Section II) and the relevant orders of magnitudes of the current amplitudes and frequencies, as well as numbers of fibers of the microfiber rings (Section III). In the main part of the paper, we develop the relevant theory (Section IV) and support and illustrate the findings with experimental results (Sections V and VI, for experimental setup and results, respectively). Because of the many different aspects influencing these characteristics, both the discussion of the theory and of the experimental results is organized in several sections, each focusing on another aspect of the current-carrying characteristics. In many applications, these numerous different parameters lead to a complex

overall situation. By identifying and quantifying the important tendencies that affect the microfiber ring characteristics, the paper provides an understanding of the concept and the design aspects for such HF electric contacts. These are summarized in a comprehensive way in the conclusions at the end of the paper, bringing together the different subsections of and aspects discussed within the paper.

## II. REVIEW: MICROFIBER RING CONCEPT

Conductive microfiber rings are made from millions of conductive microfibers [see Figs. 1(a) and (b)], giving a high density of contact points to establish the electric contact between two conductive elements, one at rest, and one moving (in most cases rotating). These fibers have strands less than one denier [1 denier = 1 g/(9000 m of fiber)], very small diameters of less than  $10\ \mu\text{m}$  [see Fig. 1(c)], and are mechanically flexible and yet high strength, high stiffness fibers. In the case of the application discussed in this paper—rotating machinery—the fibers are aligned radially to the shaft and cover the whole circumference. If applied with the correct interference, these rings can maintain contact with the surface, compensating surface roughness, and/or microscopic variations of the distance resulting from nonideal centering/alignment and cutting through any layers of contamination on the sliding interface. When the microfibers lose “good” electric contact by mechanical contact, a breakdown due to local field emission will occur somewhere along the circumference, thereby reestablishing the electric contact. The above quoted negligible frictional wear has been shown by no such wear reported on more than  $10^5$  microfiber rings presently installed in the field, where more than  $10^4$  among these have been operating for over four years. In a laboratory test, only  $25\ \mu\text{m}$  of wear have been observed on a microfiber ring for 25.4 mm (1 in) shaft diameter continuously running at 3600 r/min for one year of operation. Such small wear requires that the microfiber fit is correctly designed. Notably, in applications with change of direction of rotation, the fiber deflection and bending during reversal of the direction of rotation need to be within the limits of elastic deformation of the microfibers.

TABLE I  
RANGES OF CURRENT AMPLITUDES UNDER CONSIDERATION [25]

$dv_{lg}/dt$ kV/ $\mu$ s	$C_{wf}^{(1)}$ nF	$I_{com}^{(avg)}$ A	$I_b = 0.1I_{com}$ A	$I_b = 0.35I_{com}$ A
0.5	2...30	2...30	0.2...3.0	0.7...10.5
1.0	2...30	4...60	0.4...6.0	1.4...21
2.0	2...30	8...120	0.8...12	2.8...42

<sup>(1)</sup>Phase value,  $I_{com} = 2 \cdot C_{wf} \cdot dv_{lg}/dt$ .

### III. REVIEW: ORDERS OF MAGNITUDES

#### A. Current Amplitudes and Frequencies

As an application of conductive microfiber electrical contacts, we select the field of inverter-induced bearing currents occurring with “large” drives of several hundred kilowatt rated power as application to identify the orders of magnitudes of the current amplitudes and frequencies to be carried by the microfiber rings. If used in this context, the microfiber rings are required to carry either ground ( $i_{com}$ , also: “common mode”) or HF circulating bearing currents ( $i_b$ ). These currents have frequencies of up to several megahertz. For the amplitudes of  $i_{com}$  and  $i_b$ ,  $I_{com}$  and  $I_b$ , respectively, we refer to the simplified estimations carried out in [25] and recapitulate the results in Table I, where  $dv_{lg}/dt$  is the  $dv/dt$  of the voltage between the motor terminal connection (“line”) and the ground and  $C_{wf}$  is the stator winding-to-frame capacitance. From the table, it becomes clear that the microfiber rings can easily be required to carry currents of several tens of amperes.

#### B. Number of Fibers

Similar to above, we recapitulate results presented in [25] to show the orders of magnitudes of the numbers of fibers. Here, we approximate the fiber current density with  $10^{10}$  A/m<sup>2</sup>, using [26] as a starting point and assuming that only (1...10)% of the multitude of fibers assembled in parallel carry current at the same time, because of the nonuniform contact between the microfibers and the surface throughout the brush contact area resulting in different contact resistances and thus nonuniform distribution of the currents through the fibers. Then,  $10^5$  fibers can carry (0.78...7.8) A and  $10^6$  fibers can carry (7.8...78) A respectively. In general, a high ratio between the number of fibers of a given microfiber ring and the current flowing through it will lead to a lower percentage value of the fibers carrying current.

#### C. Further Analysis

For the values derived above, it is important to note that the value  $10^{10}$  A/m<sup>2</sup> is the value where it was observed that the field emission current diverged from the Fowler–Nordheim equation (1 mm contact gap), which was attributed to the effect of space charges reducing the field at the emitter [26], [27]. This value had been taken to estimate the number of fibers because of the role of field emission for their proper functioning, but it had not been derived from studies of the thermal heat developed. The continuous reversal of the electromagnetic field as it occurs with AC currents and voltages—which are in the focus of this paper—will further increase the current-carrying capabilities of the microfibers (see below, Section IV-C). It is

important for the microfiber rings to have a sufficiently high current-carrying capability for the corresponding application. However, this criterion should not obscure the other important aspect influencing the choice of the number of fibers: for a given circumference, a “sufficiently” high number of fibers is required to cut through any layer of contamination on the sliding interface and to compensate the deviation from the true roundness of the shaft, leading to a decreasing ratio between current and number of fibers and lower percentage of fibers carrying current at a given time with increasing shaft diameter.

### IV. THEORY

#### A. Introduction

The current-carrying characteristics of the microfiber rings are strongly determined by the resistance of the fiber assembly, including its contact with the shaft. The resistance of an individual fiber,  $R_{f1}$ , is a function of the current through the fiber and the contact between the fiber and the moving surface of the rotating shaft, notably since field emission and ionization can take place due to the occurrence of locally very high electric fields. In the following, we first consider the ohmic resistances and then include the influences of the current characteristics and the shaft rotation into the theoretical explanations developed.

#### B. Ohmic Resistance of the Fibers

1) *Introductory Remarks:* To calculate the ohmic fiber resistance, we distinguish between the fiber shaft resistance and the constriction resistance at the fiber tip. The specific resistivity  $\rho$  of electrographite material varies with its grade. According to Slade [28], common electrographitic material has a specific resistivity of  $\rho \approx 6000 \mu\Omega\cdot\text{m}$ , but lower values can be found as well with higher grade material as, for example, used in conventional carbon brushes, e.g.,  $\rho \approx (18 \dots 100) \mu\Omega\cdot\text{m}$  [29] and  $\rho \approx (9 \dots 90) \mu\Omega\cdot\text{m}$  [30]. Values more than one magnitude smaller can be achieved with use of metal–graphite material. The material used for the fibers of the microfiber rings described here has a specific resistivity of  $\rho \approx 18 \mu\Omega\cdot\text{m}$ . In analogy to the conventional brushes, the fibers can also be coated with copper, whereby specific resistivities as low as  $\rho \approx 0.0175 \mu\Omega\cdot\text{m}$  can be obtained. In order to illustrate the huge range of obtainable values, we quantify the microfiber ohmic resistance for all three classes of the specific resistivity.

2) *Influence of the Frequency—Eddy Current Effects:* At the small diameters of the fibers, and considering an upper bound of the current frequency of several megahertz, eddy current effects are negligible. Even for 10 MHz and copper, which has an “ideal conductivity” when compared to the microfibers and thereby provides a lower bound for the investigations reported on here,  $\rho_{cu} \approx 0.0168 \mu\Omega\cdot\text{m}$ , the skin depth is still  $\delta \approx 20 \mu\text{m}$ . A similar analysis, but using a more complex formula (such as the equation to account for the increase of the resistance of bundles of litz-wire with frequency presented in [31]), has been carried out for the bundle level, confirming the above approximation.

3) *Shaft Resistance:* The resistance of the fiber shaft  $R_s$  is calculated from the fiber radius  $a_s$ , length  $l$ , and specific

TABLE II

CALCULATED FIBER SHAFT RESISTANCES FOR DIFFERENT FIBER LENGTHS AND SPECIFIC RESISTIVITIES;  $R_{s,1}$ ,  $R_{s,1k}$ , AND  $R_{s,100k}$ : VALUES FOR  $10\text{ }\mu\text{m}$  FIBER DIAMETER, 1 INDIVIDUAL FIBER,  $10^3$ , AND  $10^5$  FIBERS CONDUCTING IN PARALLEL

Specific resistivity [ $\mu\Omega\text{m}$ ]	Fiber length [mm]	$R_{s,1}$ [ $\Omega$ ]	$R_{s,1k}$ [ $\Omega$ ]	$R_{s,100k}$ [ $\Omega$ ]
6000	10	763 944	764	7.639
6000	5	381 972	382	3.820
18	10	2292	2.292	0.023
18	5	1146	1.146	0.011
0.0175	10	2.228	$2.2 \cdot 10^{-3}$	$2.2 \cdot 10^{-7}$
0.0175	5	1.114	$1.1 \cdot 10^{-3}$	$1.1 \cdot 10^{-7}$

TABLE III

CALCULATED CONSTRICTION RESISTANCES FOR DIFFERENT SPECIFIC RESISTIVITIES;  $R_{c,1}$ ,  $R_{c,1k}$ , AND  $R_{c,100k}$ :  $10\text{ }\mu\text{m}$  FIBER DIAMETER, 1 INDIVIDUAL FIBER,  $10^3$ , AND  $10^5$  FIBERS CONDUCTING IN PARALLEL

Specific resistivity [ $\mu\Omega\text{m}$ ]	$R_{c,1}$ [ $\Omega$ ]	$R_{c,1k}$ [ $\Omega$ ]	$R_{c,100k}$ [ $\Omega$ ]
6000	$6 \cdot 10^2$	$6 \cdot 10^{-1}$	$6 \cdot 10^{-3}$
18	$1.8 \cdot 10^0$	$1.8 \cdot 10^{-3}$	$1.8 \cdot 10^{-5}$
0.0175	$1.75 \cdot 10^{-3}$	$1.75 \cdot 10^{-6}$	$1.75 \cdot 10^{-8}$

resistivity  $\rho$ ,

$$R_s = \rho \frac{l}{\pi a_s^2}. \quad (1)$$

The resistance of the fiber shaft per unit fiber length  $R'_s$  can easily be derived from (1). For  $\rho = (0.0175, 18, 6000)\text{ }\mu\Omega\text{-m}$  (corresponding approximately to coated fibers, uncoated fibers, and conventional material, respectively) and  $10\text{ }\mu\text{m}$  fiber diameter, it is  $R'_s = (2.23, 2292, 763\,944)\text{ }\Omega/\text{cm}$ , respectively. A summary of the resulting practically relevant ranges of  $R_s$  for fiber lengths 5 and 10 mm is given in Table II, where we consider both individual fibers, and  $10^3$  and  $10^5$  fibers conducting in parallel. The range of obtainable values is huge, including values as high as several hundred ohms for conventional material, a few ohms for uncoated fibers, and values as low as a few milliohms for coated fibers, all for  $10^3$  fibers conducting at the same time. With  $10^5$  microfibers conducting in parallel, the values are by a factor of 100 smaller. Note also that the number of fibers conducting in parallel is not equal to the number of fibers of the microfiber ring, because only a small fraction of the fibers will be conducting at a given time, as described previously (see Section III-B).

4) *Constriction Resistance:* Next, we calculate the constriction resistance  $R_c$ , where we assume that the contact is at rest. The influence of the rotating shaft and thus moving contact surface will be discussed below (see Section IV-D). With the contact spot radius  $a_c$ , it is [26]

$$R_c = \frac{\rho}{2a_c}. \quad (2)$$

Similar to above, a summary of the resulting practically relevant ranges of  $R_c$  is given in Table III. Note that  $R_{c,a_c=a_s} \ll R_{c,a_c < a_s}$  even for the case that the radius of the contact area  $a_s$  is much smaller than the one of the fiber cross-sectional area  $a_c$ .

5) *Conclusions:* Comparing the expressions for  $R_c$  and  $R_s$ , we obtain

$$\frac{R_s}{R_c} = \frac{\rho l / (\pi a_s^2)}{\rho / (2a_c)} = \frac{2}{\pi} \frac{l a_c}{a_s^2} = \frac{2}{\pi} \frac{l}{a_s} \frac{a_c}{a_s}. \quad (3)$$

Since  $l$  is in the order of several millimeters and  $a_s$  of some ten micrometers, we approximate  $l \geq 500 a_s$ . Furthermore,  $a_s \geq a_c$  and we obtain as a lower bound,

$$\frac{R_s}{R_c} \geq \frac{2}{\pi} \cdot 500 \cdot 1 = 318. \quad (4)$$

It becomes clear that the relative contribution of the individual resistance components  $R_s$  and  $R_c$  to the overall fiber resistance  $R_f$  depends on: 1) the ratio of the fiber length to its shaft diameter and 2) the truncation at the fiber tip. However, the contribution of the shaft resistance  $R_s$  is much larger than the one of the constriction resistance  $R_c$ . Furthermore, it is important to note that small fiber tips are only required to enable field emission leading to voltage breakdowns already at low voltages, thereby initiating current flow and the built-up of current conducting bridges under the corona effect. Therefore, “relatively large” contributions of  $R_c$  at small fiber tips are only effective while the current-conducting paths are being formed. In addition, current-conducting “bridges” will establish at the point of contact through field emission and ionization (see Section IV-C). This will significantly reduce the effectiveness of the constriction resistance. As a result, the contribution of  $R_c$  toward  $R_f$  is considered negligible, and  $R_{f,1}$  can be computed from (1).

### C. Influence of Field Emission and Ionization

In the presence of a high electric field, field emission and ionization can occur and the microscopic field strength at the microsurface of the contact can be several orders larger than the macroscopic one. For more detailed explanations and data, see [32]–[37] as well as [24] and [25], where we have shown how this effect can be exploited to discharge even small voltages of a few volts. Such discharges occur when the electrons resulting from field emission can initiate an electric breakdown when the (local) field emission current density (at microscopic level) exceeds a critical value [26]. The power behind the discharged voltage permitting, currents will flow through the newly established electric contact. These currents are orders of magnitudes larger than those due to field emission that led to the electric breakdown and initiated the current-conduction process. These currents further increase the local current density and facilitate the development of current-conducting “bridges.” As the currents increase, more of such “bridges” build up, further reducing the resistance of the electric contact. If the local field becomes strong enough, the field ionization begins, whereby electrons tunnel into the tip [32]. The air surrounding the fiber tips becomes ionized, allowing the charges to travel (corona effect), and the current is mainly determined by the supply function. Under these conditions, the fibers have “good” current-conducting properties, but the resistance is large enough to limit the current amplitudes caused by the voltage source behind the current to values the fibers can carry.

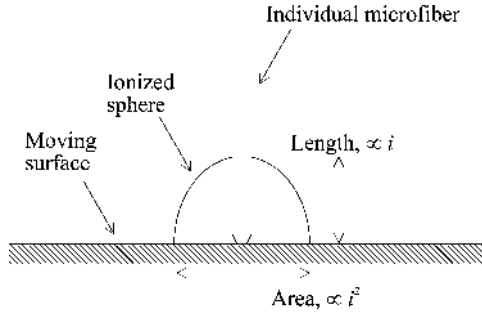


Fig. 2. Illustration of the understanding of the ionized field at the tip of the microfiber from which (5) is derived. (Not to scale. Only one fiber shown and curvature of the surface neglected.)

As of a certain critical current density, impact ionization and Townsend avalanche take place leading to a “collapse” of the current conduction. The current amount must be limited to values below this threshold to maintain the fiber integrity, since the fiber tips that are engaged with the avalanche reach a very high temperature above the melting point of the fiber. This phenomenon is not further discussed here, because it is hardly only relevant with dc and low-frequency currents. With the HF currents discussed here, the continuous reversal of the direction of flow of the physical current, and thus, of the electrons counteracts this effect. This leads to much higher current conducting abilities for HF than DC and low-frequency currents. The current-carrying capabilities of a given number of fibers discussed above (see Section III-B) is therefore a conservative estimate and a lower bound for HF applications.

To quantify the influence of the current magnitude on the value of the resistance, we consider the change of the height (which is the length the current passes through) and of the area of the ionized field (and hence of the current-conducting “bridges”) at the fiber tip the current passes through (see Fig. 2). Both parameters will increase with the current magnitude  $i$  because of the corresponding widening of the field, where the change of the area will be larger than the one of the length. If the ionized field has the form of a sphere, the length will increase  $\propto i$  and the area  $\propto i^2$ . The resistance  $R$  is proportional to the length and to the inverse of the area and thus is in the case of the sphere approximately  $\propto 1/\sqrt{i}$ . For the more general case, we therefore describe the microfiber resistance by

$$R_f = \frac{c_1}{i^{c_2}}. \quad (5)$$

The proportionality constant  $c_1$  corresponds to the resistance at one ampere current and will be in the order of the purely ohmic resistance determined above (see Section IV-B) and  $c_2$  will be in the range  $0 < c_2 < 1$  as just derived. Both coefficients depend on the current frequency and shaft speed as discussed in the following (see Section IV-D and IV-E).

#### D. Influence of the Shaft Speed

The electric contact between an individual fiber and the machine shaft would not be influenced by the speed of the latter if the moving surface of the rotating shaft had infinite conductivity and were infinitively smooth. In this ideal case, electrons could

instantaneously follow the point of contact of an individual fiber at the shaft surface and the current-conducting bridges would not have to reform themselves under the influence of the surface roughness. However, in practice, the bridges can tear off as the fiber is engaged with the moving surface. In order to improve the surface to become closer to a conductive ideal smooth surface, a conductive coat from silver paste can be applied to the shaft surface. In addition, such a coat can both prevent surface oxidation (that would counteract the field emission properties) and other nonconductive material filling into the low spots of the rotating surface.

To assess the conditions for “good” electric contact to exist, we first consider the time for a current-conducting bridge to develop,  $t_b$ , the distance the fibers travel during this time,  $s_b = v \cdot t_b$ , with the velocity at the shaft surface  $v$ , and the length of the contact area along the circumference, which corresponds approximately to the fiber diameter  $2a$ . As the speed of the machine shaft increases, the ratio  $s_b/(2a)$  increases, where  $s_b/(2a) \ll 1$  is required to ensure good electric contact (see Fig. 3). The surface speed ranges from 0.5 to almost 30 m/s for motor speed of (180 . . . 3600) r/min and shaft diameters between 50 and 150 mm. Selected ratios  $s_b/(2a)$  for  $t_b = 1, 0.1$ , and  $0.01 \mu\text{s}$  are summarized in Table IV. The chosen values of  $t_b$  represent the upper and lower bounds of relevant times  $t_b$ . From the table, it becomes clear that the selection of the fiber diameter clearly is a tradeoff between: 1) good field emission (truncate tips, low breakdown voltages, small  $t_b$ ) and 2) good electric contact following the breakdown ( $s_b/(2a) \ll 1$ ) as well as a low resistance  $R_s$ . At sufficiently small fiber diameters and interference, the microfibers will tend to operate rather at the lower values of  $t_b$  listed and the ratios allow for good current-conduction properties.

Because the likeliness for current-conducting bridges to tear off [expressed through the ratio  $s_b/(2a)$ ] increases with the shaft speed both the coefficients  $c_1$  of  $c_2$  of (5) increase with shaft speed. The reasoning for  $c_1$  is straightforward from the negative influence of the tearing off on the resistance. Since larger currents are also less likely to tear off,  $c_2$  will also increase with shaft speed.

#### E. Influence of the Current Frequency

1) *Tearing Off of the Current-Conducting Bridges:* The highest likeliness for a current-conducting bridge to tear off occurs during zero-crossings of the currents since, assuming almost perfect ohmic behavior, the electric field is minimum at this moment. The number of zero-crossings of the current is directly proportional to its frequency, with  $2 \times 10^5 \dots 2 \times 10^7$  zero-crossings at  $f = (0.1 \dots 10)$  MHz respectively. The corresponding times between two zero-crossings,  $t_{zc} = T/2$ , with the period time  $T = 1/f$ , are  $t_{zc} = (5 \dots 0.050) \mu\text{s}$ , respectively. From  $t_{zc}$ , the distances traveled between two zero-crossings,  $s_{zc} = v \cdot t_{zc}$ , can easily be calculated. Similar to before,  $s_b/s_{zc} \ll 1$ , what is equivalent to  $t_b/t_{zc} \ll 1$ , is required to ensure good electric contact (see Table V). Again, a tradeoff has to be made during the design process, since smaller fiber diameters lead to smaller values of  $t_b$ , but increase the fiber

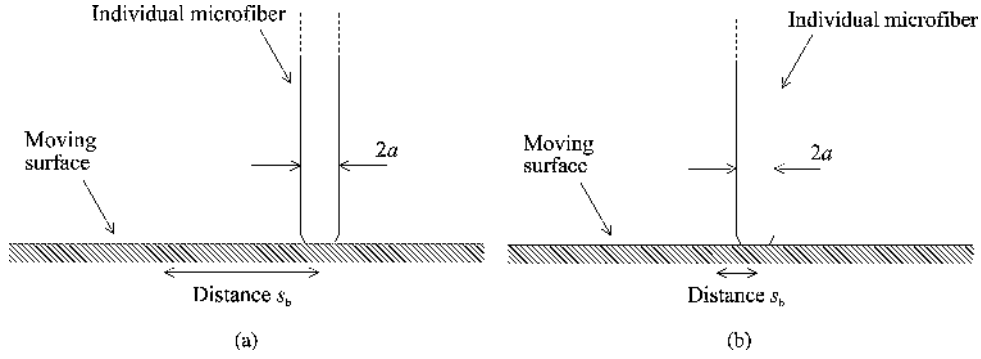


Fig. 3. Illustration of relationship between fiber diameter  $2a$  and distance  $s_b$  a microfiber travels during the time  $t_b$  that is required for a current-conducting bridge to develop. (Not to scale. Curvature of the surface neglected.) (a) Fair electric contact. (b) Good electric contact.

TABLE IV  
RATIOS OF THE DISTANCE THE FIBER TRAVEL BETWEEN THE TIME FOR CURRENT-CONDUCTING BRIDGE TO DEVELOP  $s_b$  AND THE FIBER DIAMETER  $2a$  FOR DIFFERENT SURFACE SPEED  $v$ , FOR DIFFERENT TIMES FOR A CURRENT-CONDUCTING BRIDGE TO DEVELOP  $t_b$  AND FIBER DIAMETERS

Fiber diameter [ $\mu\text{m}$ ]	Surface speed $v$ [m/s]	$s_b/(2a)$ for $t_b = 1 \mu\text{s}$	$s_b/(2a)$ for $t_b = 0.1 \mu\text{s}$	$s_b/(2a)$ for $t_b = 0.01 \mu\text{s}$
20	1	$5 \cdot 10^{-2}$	$5 \cdot 10^{-3}$	$5 \cdot 10^{-4}$
20	10	$5 \cdot 10^{-1}$	$5 \cdot 10^{-2}$	$5 \cdot 10^{-3}$
20	20	1	$5 \cdot 10^{-1}$	$1 \cdot 10^{-2}$
10	1	$1 \cdot 10^{-1}$	$1 \cdot 10^{-2}$	$1 \cdot 10^{-3}$
10	10	1	$1 \cdot 10^{-1}$	$1 \cdot 10^{-2}$
10	20	2	$2 \cdot 10^{-1}$	$2 \cdot 10^{-2}$

TABLE V  
RATIOS OF THE TIME FOR A CURRENT-CONDUCTING BRIDGE TO DEVELOP  $t_b$  AND THE TIME BETWEEN TWO ZERO-CROSSINGS  $t_{zc}$  OR THE TIME BETWEEN TWO MAXIMA OF THE SOURCE BEHIND THE CURRENT AT MAXIMUM FIELD STRENGTH  $t_{mm}$  FOR DIFFERENT CURRENT FREQUENCIES AND VALUES OF  $t_b$

Frequency [Hz]	$t_{zc}$ or $t_{mm}$ [ $\mu\text{s}$ ]	$t_b/t_{zc}$ or $t_b/t_{mm}$ for $t_b = 1 \mu\text{s}$	$t_b/t_{zc}$ or $t_b/t_{mm}$ for $t_b = 0.1 \mu\text{s}$	$t_b/t_{zc}$ or $t_b/t_{mm}$ for $t_b = 0.01 \mu\text{s}$
$10^4$	50	$2 \cdot 10^{-2}$	$2 \cdot 10^{-3}$	$2 \cdot 10^{-4}$
$10^5$	5	$2 \cdot 10^{-1}$	$2 \cdot 10^{-2}$	$2 \cdot 10^{-3}$
$10^6$	0.5	2	$2 \cdot 10^{-1}$	$2 \cdot 10^{-2}$
$10^7$	0.05	20	2	$2 \cdot 10^{-1}$

resistance  $R_f$ . Before drawing more conclusions on the influence of the frequency on the current-carrying characteristic of the microfiber rings, the reestablishment of current-conducting bridges described next also needs to be considered.

2) *Reestablishment of Current-Conducting Bridges*: In analogy to the line of argument made above, the highest likelihood for a current-conducting bridge to establish itself is during the maximum of the source behind the current at maximum electric field strength. For a given frequency, the time between two of these maxima,  $t_{mm}$ , equals the time between two zero-crossings  $t_{zc}$ . In contrast to the above case of the tearing off of the current-conducting bridges, we seek  $t_b/t_{mm} \gg 1$  for good current-conducting properties.

3) *Two Competing Factors of Influence—Conclusions*: Both the “negative influence” of the zero-crossings and the “positive influence” of the similarly increasing number of maxima of the source behind the current at maximum field strength

increase with frequency. The source behind the current is always present, whereas any nonideal contact at the interface due to surface roughness will only affect the contact statistically distributed. Therefore, the second aspect—reestablishment of current-conducting bridges—will have a stronger influence with increasing frequency than the first—tearing off of the current-conducting bridges, and the resistance will decrease with increasing frequency. Therefore,  $c_1$  of (5) will decrease with frequency as “good” electric contact is enhanced, whereas  $c_2$  will increase because the influence of the number of electrons passing through the contact within a given time (expressed as the current magnitude) is stronger where less time is available for the air surrounding the fibers to become ionized. It needs mentioning that applications may also require electric contact established for signals that contain a spectrum of different frequency components instead of a single frequency component. For such cases, the resistance of the microfiber ring cannot be computed as a superposition of the resistances for the individual frequency components but depends on the magnitude in the time domain and the effective moments of zero-crossing and of maximum electric field strength of these signals. Because of the added complexity and the relative small influence of the frequency when compared to other parameters (see below), the detailed analysis of these relationships is beyond the scope of this paper. However, our approach allows to identify an envelope of the behavior and the identification of tendencies that are satisfactory to estimate the general characteristics of conductive microfiber rings. The true characteristic will lie in-between these extremes, as has also been observed in field experiments and measurements carried out in a slightly different context (see the report on the mixed signals in [25]).

## V. EXPERIMENTAL SETUP

### A. Test Setup

A test setup was constructed to measure the HF current-conduction capability of microfibers. To this aim, two microfiber rings were installed on a rotating shaft made from aluminum that was electrically isolated from the motor shaft and on an electrically isolated test bench. The shaft diameter was increased to 100 mm (3.94 in) using an aluminum cylinder on which a coat from silver paste was applied to improve the

TABLE VI  
SELECTED DATA OF TEST SETUP AND MICROFIBER RINGS UNDER TEST

Shaft diameter	100 mm (3.94 in)
Shaft material	aluminum
Coating material	conductive silver
Coating thickness	0.025 mm (0.001 in)
Inner diameter of ring (incl. fibers)	98.45 mm (3.88 in)
Outer diameter of ring	129.5 mm (5.1 in)
Width of ring	0.464 mm (0.018 in)
Separation between rings	30.02 mm (1.18 in)
Total number of fibers per ring	2 574 000
Fiber type	uncoated

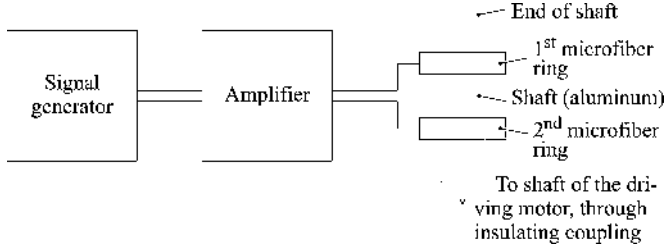


Fig. 4. Sketch of test setup for the measurement of the microfiber ring HF current-conduction characteristics.

surface current-conducting properties. The data of the test setup and microfiber rings under test are summarized in Table VI. The two microfiber rings were connected in series on the shaft and voltage was applied to the rings (see Fig. 4). Sine wave signals up to 10 MHz were applied using a 10 MHz signal generator and a 10 kHz to 10 MHz, 1 kW power amplifier. The currents and voltages were measured with the help of a 50 MHz current probe, 500 MHz voltage probes, and a 600 MHz, 5 GS/s scope [see Figs. 5(a) and (b)], taking the appropriate measures for such HF investigations. The upper frequency limit of the experimental tests of 10 MHz was given by the availability of an amplifier with both an appropriate frequency and power range. In addition, an internal control mechanism of the amplifier limited the current amplitude depending on the frequency. Despite these limits, the measurements cover a wide enough range of operating conditions to support the theoretical investigation. To our knowledge, this is the first time measurement results on current-conduction properties of brushes up to such high frequencies (and with “reasonably large” current amplitudes) are shown. They thereby contribute to the development and use of alternative current-conducting mechanisms across sliding surfaces, notably for HF applications with larger current amplitudes.

### B. Microfiber Rings under Test

Each of the microfiber rings under test (see Fig. 6) had 2 574 000 uncoated fibers with  $7 \mu\text{m}$  fiber diameter, and hence,  $R'_s = 18 \Omega \cdot \text{cm} / \pi (3.5 \mu\text{m})^2 = 4 677 \Omega / \text{cm}$ . The fibers are sandwiched between two aluminum plates with different inner diameters. On one side, the fiber length protruded beyond the aluminum plate inner diameter is 4 mm; on the other side, it is 9.8 mm. Since the resistance is linear with length, and individual points of contact between the individual microfibers exist, we use an average fiber length of 6.9 mm for our calculations

and obtain a fiber shaft resistance per fiber of  $R_{s,1} = 3 227 \Omega$ . If all 2 574 000 fibers would be conducting in parallel, this would result in an overall resistance of  $R_{s,\text{ring},100\%} = 0.0013 \Omega$ . However, as discussed above (see Section III-B), we assume that only  $(1 \dots 10)\%$  of the fibers are conducting at the same time, resulting in  $R_{s,\text{ring},(1 \dots 10)\%} = (0.1254 \dots 0.0125) \Omega$ .

### C. Other Resistances

The contribution of the resistance of the aluminum shaft between the two microfiber rings  $R_{\text{al,shaft}}$  is calculated from the distance between the two microfiber rings under tests  $d_{2\text{mfrs}}$ , the skin depth  $\delta_{\text{al}}$ , the shaft diameter  $d_{\text{shaft}}$  and the specific resistivity of aluminum  $\rho_{\text{al}} = 0.0265 \mu\Omega \cdot \text{m}$ ,

$$R_{\text{al,shaft}} = \rho_{\text{al}} \frac{d_{2\text{mfrs}}}{\delta_{\text{al}} \pi d_{\text{shaft}}} = 0.0265 \times 10^{-6} \Omega \cdot \text{m} \cdot \frac{0.03 \text{ m}}{\delta_{\text{al}} \pi 0.1 \text{ m}}. \quad (6)$$

Since this resistance increases with frequency (decreasing  $\delta_{\text{al}}$ ), the highest contribution toward the measured resistance occurs at 10 MHz. However,  $R_{\text{al,shaft},10 \text{ MHz}} \approx 0.0001 \Omega \ll R_s$ , and we therefore neglect this contribution when compared with the one of the microfibers themselves.

In analogy, we also estimate the contribution of the aluminum ring of the microfiber rings to the total measured resistance  $R_{\text{al,ring}}$ . The length the current passes through is approximately 8 mm, the area is  $\delta_{\text{al}} \pi d_{\text{al}}$ , with the average diameter of the aluminum ring  $d_{\text{al}}$ . Since  $d_{\text{al}} \approx 112 \text{ mm} \approx d_{\text{shaft}}$  and  $8 \text{ mm} \approx 0.27 d_{2\text{mfrs}}$ , the contribution of the aluminum rings  $2 R_{\text{al,ring}}$  to the total resistance is even smaller than the one of  $R_{\text{al,shaft}}$ , and is therefore, also neglected.

## VI. EXPERIMENTAL RESULTS

### A. General Characteristic

In general, we observe scattering, notably at lower frequencies and shaft speed, indicating the interaction of surface roughness and local field breakdowns and built-up of current-conducting bridges. The ohmic behavior of the microfiber rings is clearly seen (see Fig. 7).

Depending on the current magnitude and frequency and the motor speed, the resistance per microfiber ring averages approximately  $(0.10 \dots 0.15) \Omega$ , as will be shown in more detail in the following. This value is in line with the previously computed value for 1% of the microfibers conducting at the same time ( $R_{s,\text{ring},1\%} = 0.1254 \Omega$ ; see Section V-B). Note that the low percentage of fibers conducting at a given time is in line with the theory for large microfiber rings with a very high number of microfibers (see Section III-C).

### B. Influence of the Current Magnitude

In line with the theory of increasing built-up of current-conducting bridges with increasing current magnitude (see Section IV-B), the measured resistance of the microfiber ring decreases slightly with increasing current magnitude, as illustrated in Fig. 8, using exemplarily the results for  $f = 10 \text{ MHz}$ .

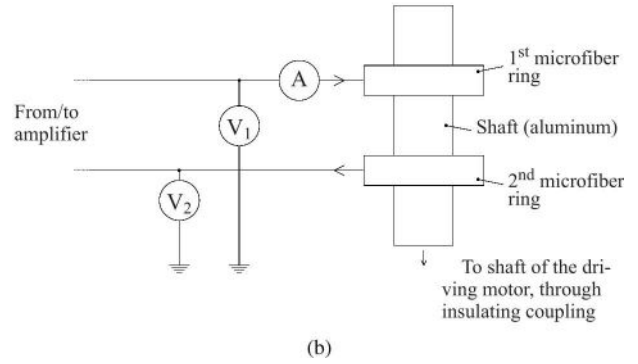
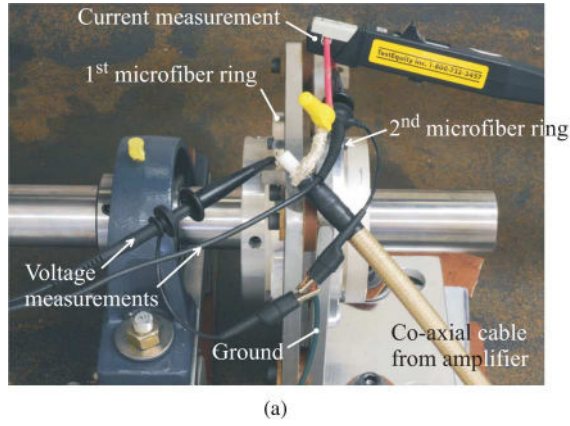


Fig. 5. Measurement of HF current-conduction characteristics of the microfiber rings under test. (a) Arrangement of microfiber rings under test installed on a rotating shaft made from aluminum, current, and voltage probes. (b) Sketch of the measurement connections.



Fig. 6. Microfiber ring under test (see Table VI) for selected data.

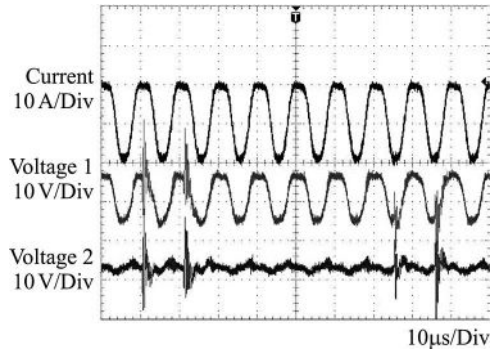


Fig. 7. Measured current through the two microfiber rings and voltage at the outer rings respectively,  $f = 100$  kHz,  $n = 900$  r/min. The voltage across the two microfiber rings is the difference between the two measured voltages. The ohmic behavior is clearly seen.

The measured characteristics are approximated by  $R_f = c_1/i^{c_2}$ , following the results of the previous theoretical analysis. The corresponding curves, equations (and hence, coefficients  $c_1$  and  $c_2$ ), and the  $R^2$ -values can also be seen in the figure. The curves fit the data very well, as expressed by the high  $R^2$ -values. Furthermore, all exponents of  $1/i$  are in the order of  $c_2 \approx 0.5$  (hence  $R_f \propto 1/\sqrt{i}$ ) as predicted. The proportionality coefficients  $c_1$  are in the range of approximately (0.2...0.5),

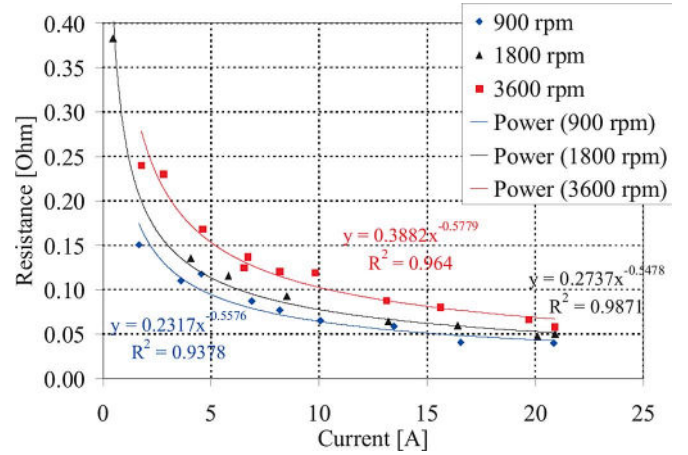


Fig. 8. Measured resistance per microfiber ring for different motor speed and current amplitudes,  $f = 10$  MHz;  $R = c_1/i^{c_2}$  approximations of the observed characteristics and corresponding  $R^2$ -values.

which is also the ohmic value of  $R_f$  at  $i = 1$  A. Considering that only a very small fraction of the more than  $2 \times 10^7$  microfibers will conduct current at a given time at such a small current ( $<1\%$ ), this is in line with the theory. Very similar  $R-i$  characteristics are also observed at the other investigated frequencies, as can be seen in Figs. 9(a)–(c) below. These will be discussed further in the next section (see Section VI-D). Also, the correlation between the individual coefficients  $c_1$  and  $c_2$  for the different shaft speed will be discussed within the corresponding paragraph (see Section VI-C).

### C. Influence of Motor Speed/Shaft Surface Velocity

First, we consider again Fig. 8, now focusing not primarily on the influence of the current, but on the differences between the three curves obtained for three different motor speed. (At the given shaft diameter, the three investigated motor shaft speed correspond to shaft surface velocities of 4.7, 9.4, and 18.9 m/s respectively.) A comparison with Table IV shows that the requirement  $s_b/(2a) \ll 1$  is still satisfied for the maximum speed ( $t_b = 0.1 \mu\text{s}$  and  $t_b = 0.01 \mu\text{s}$ ). In line with the theory (see Section IV-D), the measured resistances increase slightly

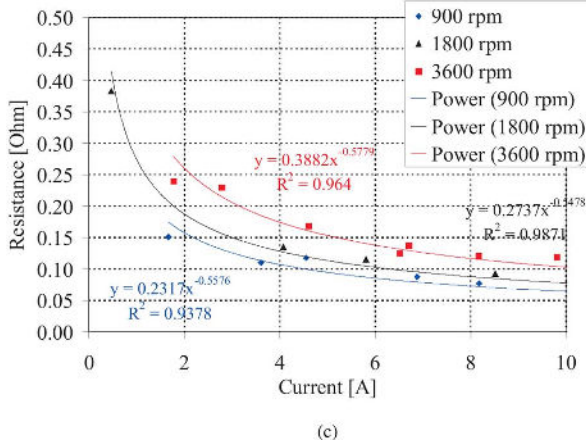
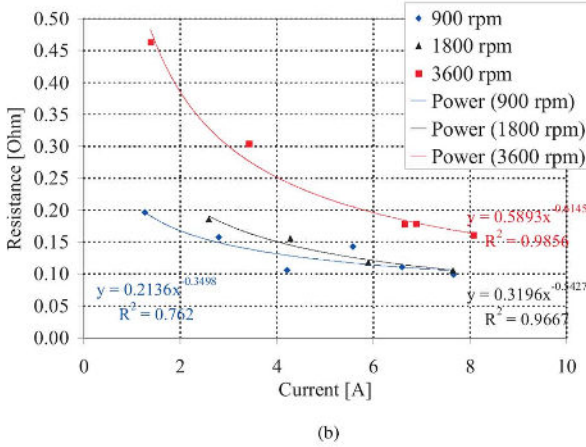
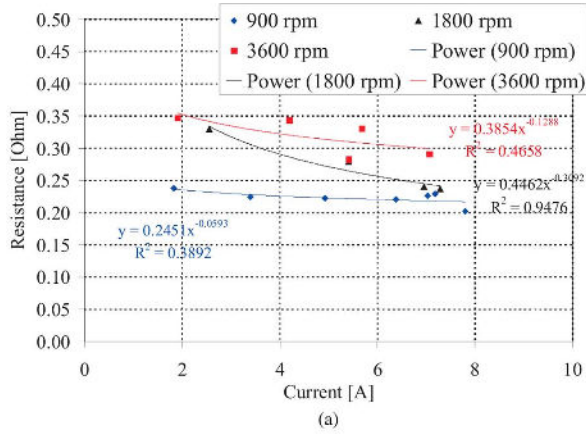


Fig. 9. Measured resistance per microfiber ring for different motor speed and current frequencies. (Same scales of current and resistance by intention.) (a)  $f = 100$  kHz. (b)  $f = 1$  MHz. (c)  $f = 10$  MHz.

with the shaft surface velocity. Regarding the coefficients of the  $R$ - $i$  curve, this translates into the predicted increase of  $c_1$  (larger value of  $R_f$  for a given current because of a higher likelihood of tearing off to occur) with motor speed. (Here,  $c_1$  increases approximately with the square-root of the motor speed, what we explain by the fact that the surface speed only affects one dimension (circumferential direction) of the two-dimensional contact area.) The coefficient  $c_2$  (stronger counteracting effect of the current magnitude on the tearing off, enhance the contact) increases only very slightly with motor speed.

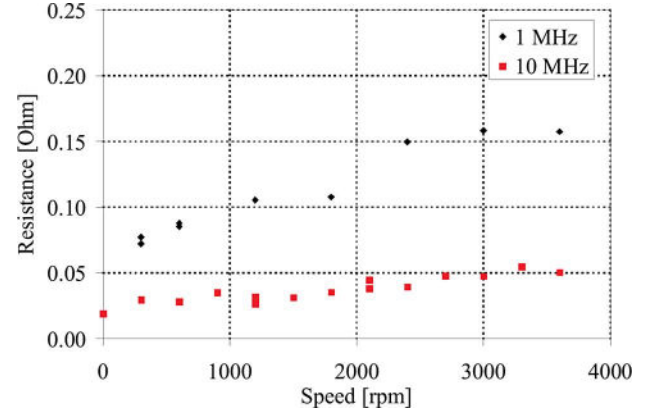


Fig. 10. Measured influence of the motor speed on the microfiber ring resistance at two different frequencies; 1 MHz:  $i \approx 4.8$  A, 10 MHz:  $i \approx 21$  A.

Next, we consider Fig. 9(a)–(c), which show the measured resistances for three sets of measurements at three different frequencies,  $f = 100$  kHz, 1 MHz, and 10 MHz, respectively. The  $R$ - $i$  curves and  $R^2$ -values are also included. At 100 kHz, the regression is only moderate, except for the 1 MHz case, and thus, remarkably lower than at the higher frequencies. This is due to the significant scattering of the measurement results. However, the general tendencies can still be seen. Here again, the measured resistances and both coefficients  $c_1$  and  $c_2$  increase with the shaft surface velocity, where the influence on  $c_1$  is much stronger than the one on  $c_2$ . (For the discussion of the influence of the frequency, i.e., a comparison of the individual measurement sets shown in Figs. 9(a)–(c), see the next section.)

Fig. 10 shows additional measurements in which the influence of the speed on the measured resistance was directly recorded, both for 1 and 10 MHz. Unfortunately, results for the same current level at the two frequencies are not available. However, the curves still confirm the increase of the microfiber ring resistance with shaft surface speed well.

With respect to applications with frequent reversal of the direction of rotation, the current-carrying characteristics of the microfibers will change with the speed during the reversal until steady-state operation is achieved again. As the microfiber ring resistance decreases with decreasing speed, the performance of the microfiber ring will rather increase than decrease during this reversal of the direction of rotation, provided the fit of the microfibers has been designed properly to limit fiber bending within the elastic deformation during the rotation reversal.

#### D. Influence of Frequency

We consider again the measurement results shown in Fig. 9, now focusing on the differences between figures (a)–(c). In line with the theory (see Section IV-E), the measured resistances decrease slightly with frequency. This translates into the predicted decrease of the proportionality constant  $c_1$  (larger value of  $R_f$  for a given current) and increase of the exponential coefficient  $c_2$  (influence of the current magnitude) with frequency. Comparing with the other factors of influence, the frequency has the smallest influence on the resistance.

## VII. CONCLUSION

Rings made from millions of conductive microfibers, if designed properly, have shown to be a good electrical contact for applications that require high frequencies and high current amplitudes while minimizing the problems of excessive wear and hot-spotting/thermal wear commonly encountered with conventional sliding contacts. In this paper, we have described the current-carrying characteristics of such rings for high frequencies up to several megahertz and large current amplitudes of several tens of amperes, thereby contributing to the development and use of alternative current-conduction mechanisms across sliding surfaces.

The theory to understand these characteristics, and thus, the ring design includes the ohmic resistance of the fiber shafts, theory of field emission and ionization, as well as the influence of the moving surface and current frequency, where the latter two can affect the possibility for “good” electric contact to exist and the development, tearing off, and reestablishment of the current-conducting paths. It has become clear that the design requires a tradeoff to be made between: 1) good field-emission properties, and thus, low breakdown voltages and 2) good electric contact following the breakdown. First, the number of fibers of a fiber ring has to be selected to meet the current-carrying requirements. Then, it needs to be ensured that the fiber density at the contact surface is “sufficiently” high and the fibers are sufficiently short to cut through any layers of contamination on the sliding interface and that the fibers have optimum lengths to minimize mechanical wear while maintaining good electric contact. With increasing ring diameter, the “cutting-through-contamination” argument becomes relatively more important than the current-carrying ability. Next, the ohmic resistance at currents of a few amperes can be determined. When doing so, it is important to consider that only a small fraction of the microfibers will carry current at a given time. This value decreases with increasing microfiber ring diameter. With a sufficient number of fibers of a few millimeter length, values in the order of a few hundred milliohms can be achieved. It should be noted that the number of fibers and their length leading to such values is often determined to ensure the mechanical properties of the sliding contact, provided material with good electric conductivity is used. With increasing current amplitude, the resistance of the microfiber rings decreases because of the increasing influence of the current-conducting bridges building up at the contact zone. This  $R$ - $i$  behavior can be approximated by  $R = c_1/i^{c_2}$ , where  $c_1$ —the ohmic value of the resistance at one ampere current—is in the order of a few hundred milliohms and  $c_2$ —the decrease of the resistance with current magnitude—is in the order of 0.5. Considering the influences of the shaft speed and frequency, respectively, the resistance increases with the first and decreases with the latter. The likeliness for current-conducting bridges to tear off increases with motor speed and the likeliness for the microfibers to reestablish good electric contact increases with frequency. The theories developed have been illustrated with experimental results. The latter cover, to our knowledge, parameters of operation never presented before in the context of electric sliding contacts. Many applications comprise a complex system of the numerous different parameters involved. This

work has identified and quantified the important tendencies that affect the microfiber ring characteristics, thereby providing an understanding of the concept, design aspects, and possibilities offered by for such HF electric contacts.

It also needs mentioning that the results obtained for HF signals can only be extrapolated to dc signals within a limited scope. For a particular application, the microfiber ring design as well as the sliding surface condition must be optimized in order to prevent Townsend avalanche and impact ionization from taking place. In addition, it should also be noted that the results presented here can be applied to applications that encompass periodic breaks of the entire contact, since the microfibers will reestablish the contact due to field emission via the field emission mechanism.

## REFERENCES

- [1] M. Swamy, K. Yamada, and T. Kume, “Common mode current attenuation techniques for use with PWM drives,” *IEEE Trans. Power Electron.*, vol. 16, no. 2, pp. 248–255, Mar. 2001.
- [2] H. Akagi and T. Doumoto, “An approach to eliminating high-frequency shaft voltage and ground leakage current from an inverter-driven motor,” *IEEE Trans. Ind. Appl.*, vol. 40, no. 4, pp. 1162–1169, Jul./Aug. 2004.
- [3] H. D. Paula, D. A. de Andrade, M. L. R. Chaves, J. L. Domingos, and M. A. A. de Freitas, “Methodology for cable modeling and simulation for high-frequency phenomena studies in PWM motor drives,” *IEEE Trans. Power Electron.*, vol. 23, no. 2, pp. 744–752, Mar. 2008.
- [4] S. Chen, T. A. Lipo, and D. Fitzgerald, “Modelling of motor bearing currents in inverter drives,” *IEEE Trans. Ind. Appl.*, vol. 32, no. 6, pp. 1365–1370, Nov./Dec. 1996.
- [5] D. Busse, J. Erdman, R. Kerkman, and D. Schlegel, “Bearing currents and their relationship to PWM drives,” *IEEE Trans. Power Electron.*, vol. 12, no. 2, pp. 243–252, Mar. 1997.
- [6] D. Busse, J. Erdman, R. Kerkman, D. Schlegel, and G. Skibinski, “System electrical parameters and their influence effect on bearing currents,” *IEEE Trans. Ind. Appl.*, vol. 33, no. 2, pp. 577–584, Mar./Apr. 1997.
- [7] D. Busse, J. Erdman, R. Kerkman, D. Schlegel, and G. Skibinski, “Characteristics of shaft voltage and bearing currents,” *IEEE Ind. Appl. Mag.*, vol. 3, no. 6, pp. 21–32, Nov./Dec. 1997.
- [8] P. Link, “Minimizing electric bearing currents in ASD systems,” *IEEE Ind. Appl. Mag.*, vol. 5, no. 4, pp. 55–66, Jul./Aug. 1999.
- [9] A. von Jouanne and H. Zhang, “A dual-bridge inverter approach to eliminating common-mode voltages and bearing and leakage currents,” *IEEE Trans. Power Electron.*, vol. 14, no. 1, pp. 43–48, Jan. 1999.
- [10] H. E. Boyanton and G. Hodges, “Bearing fluting,” *IEEE Ind. Appl. Mag.*, vol. 8, no. 5, pp. 53–57, Sep./Oct. 2002.
- [11] R. F. Schiferl and M. J. Melfi, “Bearing current remediation options,” *IEEE Ind. Appl. Mag.*, vol. 10, no. 4, pp. 40–50, Jul./Aug. 2004.
- [12] A. Muetze and A. Binder, “Don’t lose your bearings—Mitigation techniques for bearing currents in inverter-supplied drive systems,” *IEEE Ind. Appl. Mag.*, vol. 12, no. 4, pp. 22–31, Jul./Aug. 2006.
- [13] A. Muetze and A. Binder, “Calculation of circulating bearing currents in machines of inverter-based drive systems,” *IEEE Trans. Ind. Electron.*, vol. 54, no. 2, pp. 932–938, Apr. 2007.
- [14] A. Binder and A. Muetze, “Scaling effects of inverter-induced bearing currents in ac machines,” *IEEE Trans. Ind. Appl.*, vol. 44, no. 3, pp. 769–776, May/Jun. 2008.
- [15] U. T. Shami and H. Akagi, “Experimental discussions on a shaft end-to-end voltage appearing in an inverter-driven motor,” *IEEE Trans. Power Electron.*, vol. 24, no. 6, pp. 1532–1540, Jun. 2009.
- [16] U. T. Shami and H. Akagi, “Mechanism of shaft end-to-end voltage in an inverter-driven motor,” *IEEE Trans. Power Electron.*, to be published.
- [17] H. Akagi and S. Tamura, “A passive EMI filter for eliminating both bearing current and ground leakage current from an inverter-driven motor,” *IEEE Trans. Power Electron.*, vol. 21, no. 5, pp. 1459–1469, Sep. 2006.
- [18] H. Akagi and T. Shimizu, “Attenuation of conducted EMI emissions from an inverter-driven motor,” *IEEE Trans. Power Electron.*, vol. 23, no. 1, pp. 282–290, Jan. 2008.
- [19] M. L. Heldwein and J. W. Kolar, “Winding capacitance cancellation for three-phase EMC input filters,” *IEEE Trans. Power Electron.*, vol. 23, no. 4, pp. 2062–2074, Jul. 2008.

- [20] A. A. Fardoun and E. H. Ismail, "Reduction of EMI in AC drives through dithering within limited switching frequency range," *IEEE Trans. Power Electron.*, vol. 24, no. 3, pp. 804–811, Mar. 2009.
- [21] C. Henglin, Q. Zhaoming, Y. Shaoding, and C. Wolf, "Finite-element modeling of saturation effect excited by differential-mode current in a common-mode choke," *IEEE Trans. Power Electron.*, vol. 24, no. 3, pp. 873–877, Mar. 2009.
- [22] H. Akagi, H. Hasegawa, and T. Doumoto, "Design and performance of a passive EMI filter for use with a voltage-source PWM inverter having sinusoidal output voltage and zero common-mode voltage," *IEEE Trans. Power Electron.*, vol. 19, no. 4, pp. 1069–1076, Jul. 2004.
- [23] R. Lai, Y. Maillat, F. Wang, S. Wang, R. Burgos, and D. Boroyevich, "An integrated EMI choke for differential mode noise and common mode noise suppression," *IEEE Trans. Power Electron.*, vol. 25, no. 3, pp. 539–544, Mar. 2010.
- [24] A. Muetze and H. W. Oh, "Application of static charge dissipation to mitigate electric discharge bearing currents," *IEEE Trans. Ind. Appl.*, vol. 44, no. 1, pp. 135–143, Jan./Feb. 2008.
- [25] A. Muetze and H. W. Oh, "Design aspects of conductive microfiber brushes," *IEEE Trans. Ind. Appl.*, vol. 44, no. 6, pp. 1749–1757, Nov./Dec. 2008.
- [26] P. G. Slade and E. D. Taylor, "Electrical breakdown in atmospheric air between closely spaced ( $0.2\text{ }\mu\text{m}$ – $40\text{ }\mu\text{m}$ ) electrical contacts," *IEEE Trans. Compon. Packag. Technol.*, vol. 25, no. 3, pp. 390–396, Sep. 2002.
- [27] W. P. Dyke and J. K. Troyan, "Field emission, large current densities, space charge and the vacuum arc," *Phys. Rev.*, vol. 89, no. 4, pp. 799–808, Feb. 1953.
- [28] P. G. Slade, Ed., *Electric Contacts—Principles and Applications*. Boca Raton, FL: CRC Press, p. 1073, 1999.
- [29] Schunk Kohlenstofftechnik GmbH. (2008). Carbon brushes for industrial and railway application [Online]. 4 pp. Available: [http://www.schunk-group.com/sixcms/media.php/1702/02\\_Prospekt\\_10\\_14\\_engl.pdf](http://www.schunk-group.com/sixcms/media.php/1702/02_Prospekt_10_14_engl.pdf)
- [30] PanTrac GmbH. (2003). Carbon brushes for industrial and railway technology [Online]. 24 pp. Available: <http://www.pantrac.com/Produkte/PantoBrushE.html>
- [31] C. R. Sullivan, "Optimal choice for number of strands in a litz-wire transformer winding," *IEEE Trans. Power Electron.*, vol. 14, no. 2, pp. 283–291, Mar. 1999.
- [32] R. Gomer, *Field Emissions and Field Ionization* (AVS Classics in Vacuum Science and Technology). College Park, MD: AIP, 1993.
- [33] A. Wallash, "Electric breakdown and ESD phenomena for devices with nanometer-to-micron gaps," in *Proc. Int. Soc. Opt. Eng., Conf. Rel., Testing, Charact. MEMS/MOEMS II*, Jan. 2003, vol. 4980, no. 16, pp. 87–98.
- [34] R. M. Schaffert, *Electrophotography*. New York: Wiley, 1975.
- [35] A. Wallash and T. Hughbanks, "Capacitive coupling effects in spark gap devices," in *Proc. 16th Electr. Overstress Discharge (EOS/ESD) Symp., EOS/ESD Assoc.*, 1994, pp. 273–278.
- [36] R. H. Fowler and L. Nordheim, "Electron emission in intense electric fields," *Proc. R. Soc. London, Ser. A, Containing Pap. Math. Phys. Charact.*, vol. 119, no. 781, pp. 173–181, May 1928.
- [37] T. E. Stern, B. S. Gossling, and R. H. Fowler, "Further studies in the emission of electrons from cold metals," *Proc. R. Soc. London, Ser. A, Containing Pap. Math. Phys. Charact.*, vol. 124, no. 795, pp. 699–723, Jul. 1929.



**Annette Muetze** (S'03–M'04–SM'09) received the Dipl.-Ing. and Dr. Tech. degrees in electrical engineering from Darmstadt University of Technology, Darmstadt, Germany, in 1999 and 2004, and the Dipl.-Ing. degree in general engineering from the Ecole Centrale de Lyon, Ecully, France, in 1999.

During 2004, she was an Assistant Professor in the Electrical and Computer Engineering Department, University of Wisconsin-Madison, Madison. From January 2007 to March 2010, she was with the School of Engineering, University of Warwick, Coventry, U.K., first as an Assistant and then as an Associate Professor. Since April 2010, she has been the Head of the Institute of Electric Drives and Machines, Graz University of Technology, Graz, Austria, where he is also a Professor.

Prof. Muetze was the recipient of the FAG Innovation Award 2004 for her work on inverter-induced bearing currents. She was also the recipient of the National Science Foundation CAREER Award in 2005.



**H. William Oh** (M'03) received the B.Sc. degree from Pusan National University, Pusan, Korea, in 1982, and the M.Sc. degree from Korea Advanced Institute of Science and Technology, Seoul, Korea, 1984, both in mechanical engineering.

From 1985 to 1988, he was with the University of Massachusetts, Amherst. He is currently the General Manager of Electro Static Technology, a division of Illinois Tool Works (ITW), Mechanic Falls, ME. He is the Inventor of the AEGIS SGR Shaft Grounding Ring manufactured by Electro Static Technology. He has extensive design and application experience in rotating shaft grounding and sliding electrical contacts, specializing in the mitigation of unwanted electrical currents. He is the holder of eight patents.

Mr. Oh is a member of the Illinois Tool Works Patent Society.